

Experimental and theoretical investigations of Cr(001) surface electronic structure

L. E. Klebanoff, R. H. Victora, L. M. Falicov, and D. A. Shirley

*Materials and Molecular Research Division, Lawrence Berkeley Laboratory, Berkeley, California 94720
and Departments of Chemistry and Physics, University of California, Berkeley, California 94720*

(Received 4 February 1985)

The surface electronic structure of Cr(001) is characterized by angle-resolved photoelectron spectroscopy. The spectral properties of surface-related photoemission features are found to be consistent with results from a comprehensive spin-polarized calculation of the Cr(001) surface electronic structure. The theory predicts the existence of a ferromagnetic Cr(001) surface phase characterized by a very large (3.00 electrons) surface spin polarization. The overall agreement between theory and experiment provides additional evidence that the Cr(001) surface is, in fact, ferromagnetic.

I. INTRODUCTION

Atoms at the surface of a metal have fewer nearest neighbors than their counterparts in the bulk. A fundamental electronic consequence of this reduced surface coordination is surface energy-band narrowing. As a result, any metallic property that depends critically on the valence-band width may assume different characteristics at a surface. One property that is particularly sensitive to the valence-band width is itinerant-electron magnetism.

Allan¹⁻³ was among the first to propose that energy-band narrowing at 3*d*-transition-metal surfaces might establish a surface magnetic order that was different from that of the bulk metal. The increase in kinetic energy required to populate spin-up and spin-down energy bands differentially is relatively small if these bands are narrow. Since this kinetic-energy cost may be more than offset by the additional (negative) exchange energy gained in the magnetization, there is an increased tendency toward ground-state magnetism at 3*d*-transition-metal surfaces. The experimental and theoretical study of this phenomenon for Cr(001) is the subject of this investigation.

Angle-resolved photoelectron spectroscopy (ARPES) has proved to be a powerful technique for the investigation of valence electronic structure. Peaks in an ARPES spectrum are produced by direct (or vertical) transitions in wave-vector space:⁴

$$\mathbf{k}_i + \mathbf{g} = \mathbf{k}^f. \quad (1)$$

Here \mathbf{k}_i is the wave vector (in the first Brillouin zone) of the initial state responsible for the spectral peak, \mathbf{g} is the reciprocal-lattice vector supporting the transition, and \mathbf{k}^f is the wave vector (outside the first Brillouin zone) of the final-state photoelectron in the solid.

One generally wants to extract valence-band dispersion relations $E(\mathbf{k}_i)$ from the ARPES spectra. The initial-state energy E is usually equated with the spectroscopic binding energy E_{IN} (referenced to the Fermi level, E_F) of the spectral peak. To obtain \mathbf{k}_i for the spectral peak, one must relate the photoelectron wave vector measured at the detector, \mathbf{p}^f , to \mathbf{k}^f . The wave-vector component perpen-

dicular to the surface of the photoelectron in the solid k_{\perp}^f can be determined from the perpendicular component measured at the detector, p_{\perp}^f . This determination requires an assumed final-state dispersion relation that accounts for refraction effects.⁵ The component k_{\perp}^f is therefore approximately inferred from p_{\perp}^f . For a specular surface and in the absence of surface umklapp, the final-state wave-vector component parallel to the surface \mathbf{k}_{\parallel}^f is directly measured:⁵ $\mathbf{k}_{\parallel}^f = \mathbf{p}_{\parallel}^f$. This permits an accurate determination of the initial-state wave-vector component parallel to the surface \mathbf{k}_{\parallel} via the relation:

$$\mathbf{k}_{\parallel}^f = \mathbf{k}_{\parallel} + \mathbf{g}_{\parallel}. \quad (2)$$

In Eq. (2), \mathbf{g}_{\parallel} is the component parallel to the surface of the reciprocal-lattice vector supporting the photoelectric transition. In the case of Cr(001), \mathbf{g}_{\parallel} is equivalent to a surface reciprocal-lattice vector.

For surface valence-band structure, \mathbf{k}_{\parallel} is the only meaningful quantum number. Consequently, ARPES measurements of these states can provide a very direct measurement of surface $E_{IN}(\mathbf{k}_{\parallel})$ relations. Furthermore, when plane-polarized radiation is used in the ARPES measurement, dipole selection rules⁶ can be used to assign the symmetries (group representations) of the surface initial states responsible for the ARPES spectral peaks.

The deviation of the surface magnetism from bulk behavior is thought to depend on the particular element and surface. Iron and nickel are ferromagnetic in their bulk. At their surfaces, this ferromagnetism is predicted to be enhanced.⁷⁻⁹ The surface magnetism is characterized by increased surface magnetic moments as well as by magnetic surface states and resonances.⁷⁻⁹ Recent ARPES investigations of Fe and Ni surfaces^{10,11} have provided the binding energies and symmetries of ferromagnetic surface states. The comparison of these experimental results with the latest theoretical treatments of surface electronic structure has provided great insight into the origin of surface magnetism.

A most extraordinary example of surface magnetism would be the existence of surface ferromagnetism on an otherwise antiferromagnetic Cr(001) crystal.^{1-3,12} Allan¹ predicted that the reduced coordination number (4) for the (001) surface atoms would produce energy-band narrow-

ing, resulting in the formation of an unusual surface magnetic order. His tight-binding calculation¹ for Cr(001) predicted a *ferromagnetic surface phase* characterized by an exchange-split surface spin density of states (SSDOS), and large ($2.8\mu_B$) localized surface magnetic moments. In contrast to the predictions for Fe and Ni surface magnetism,⁷⁻⁹ the Cr(001) surface moments are thought to be *much* larger than the maximum value, $0.59\mu_B$, observed for bulk chromium.¹³ Gempel's calculation¹² confirmed these theoretical results and extended the theory to finite temperature using a spin-fluctuation formalism. His results predict the persistence of Cr(001) surface ferromagnetic order for temperatures up to 850 K, well above the bulk Néel temperature of 312 K.

A previous paper¹⁴ reported two surface-related features in a temperature-dependent ARPES study of Cr(001). In this investigation, we extend the experimental and theoretical characterization of the Cr(001) surface electronic structure. The experimental details of our ARPES measurements are given in Sec. II. In Sec. III we present ARPES results that reveal the symmetry and dispersion properties of Cr(001) surface electronic features. Results from a comprehensive spin-polarized theoretical treatment of the Cr(001) ground-state surface electronic structure are reported in Sec. IV. The consistency of these theoretical results with the ARPES measurements is also examined in Sec. IV. The relationship of our work to previous ARPES investigations of Cr(001) is discussed in Sec. V. Finally, our conclusions are summarized in Sec. VI.

II. EXPERIMENTAL

ARPES spectra of Cr(001) were measured at a photon energy ($h\nu$) of 21.22 eV by using a helium-discharge (HeI_α) lamp equipped with a three-element polarizer. The plane of photon polarization could be rotated continuously 360° about the photon \mathbf{k} vector. Reference will be made to our ARPES studies using synchrotron radiation. Those measurements were performed at the Stanford Synchrotron Radiation Laboratory. The electron analyzer used for all measurements was of the electrostatic 180° hemispherical-sector variety.¹⁵ The angular resolution was $\pm 3^\circ$. The total (photon and analyzer) instrumental energy resolution was maintained at 0.10 eV full width at half maximum. The electron analyzer has the capacity for independent rotation in the horizontal and vertical planes. The experimental geometry is shown in Fig. 1. Our sample manipulator provided crystal rotation about the [001] crystal normal (azimuthal rotation) and about the [100] axis (polar rotation). The sample's azimuthal angle was oriented with the low-energy electron diffraction (LEED) pattern.

For the geometry that we label *p* polarization, the crystal's (100) mirror plane (the plane defined by the [001] and [010] axes) was azimuthally oriented so as to contain the vector potential \mathbf{A} of the radiation.¹⁶ The sample's polar position was then calibrated via laser alignment and adjusted so that the \mathbf{A} vector made a 25.0° angle with the crystal normal, as shown in Fig. 1. For *s* polarization, the \mathbf{A} vector was rotated to lie perpendicular to the (100) mir-

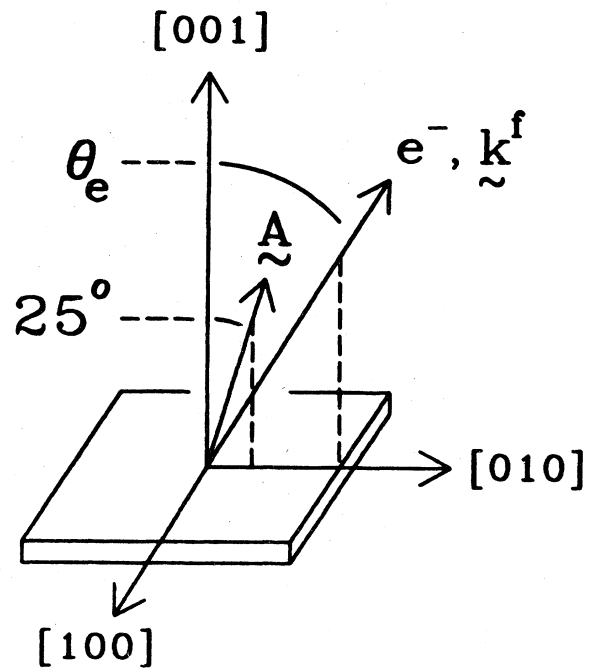


FIG. 1. The experimental geometry. The [001] direction is normal to the Cr(001) surface. The polar angle of electron detection θ_e (deg) was varied in the (100) mirror plane. The photon vector potential \mathbf{A} lies in the (100) mirror plane and makes a 25.0° angle with the surface normal. We call this photon-surface orientation *p* polarization. For *s*-polarization measurements, the \mathbf{A} vector is rotated to lie along the [100] direction perpendicular to the (100) mirror plane. All reported spectra were measured with 21.22-eV HeI_α radiation.

ror plane, along the [100] direction. ARPES spectra were collected at a variety of electron-detection angles θ_e (deg) by rotating the electron analyzer toward the [010] direction in the (100) mirror plane. Experimental angles are accurate to within $\pm 0.5^\circ$.

Our sample was a high-purity chromium single crystal that was spark-cut to within $\pm 0.5^\circ$ of the (001) plane and mechanically polished ($0.5\ \mu\text{m}$ diamond paste) to a mirror finish. As reported previously,¹⁴ the sample was argon-bombarded (5×10^{-5} Torr, 1.5 kV) with high-temperature (1120 K) cycling for three weeks to remove bulk nitrogen as detected by Auger-electron spectroscopy (AES). The crystal then displayed a very sharp, low-background (1×1) LEED pattern. No impurities were detectable by AES, or more sensitively by ARPES. Even more sensitive high-resolution electron-energy-loss spectroscopy (HREELS) measurements on Cr(001) have subsequently confirmed that this cleaning procedure produces an adsorbate-free surface.¹⁷

After an hour exposure to the residual gases in our spectrometer [pressure = 3×10^{-10} Torr (helium lamp off), 2×10^{-9} Torr (helium lamp on)], the crystal surface became contaminated with carbon and oxygen via carbon monoxide (CO) decomposition. This produced faint, blurry spots in the $c(2 \times 2)$ regions of the LEED pattern, and

an impurity (carbon and oxygen) $2p$ photoelectron peak at 6.7 eV binding energy in the ARPES spectrum. Flashing the crystal to 1120 K for 3 min removes $\sim 95\%$ of this impurity via CO desorption. This restores the low-background (1×1) LEED pattern and removes the 6.7 eV impurity peak from the ARPES spectrum. Frequent flashing of the crystal in this manner permits relatively uninterrupted study of the clean surface for 2–3 h. After this time, we argon-ion-sputtered the crystal at room temperature for 1 h to remove accumulated impurities. We then annealed the crystal at 1120 K for 5 min to restore order to the clean surface. All ARPES spectra were recorded at 298 K.

III. EXPERIMENTAL RESULTS

In this section we present ARPES measurements that extend the previous characterization¹⁴ of the Cr(001) surface electronic structure. Since chromium crystallizes in a body-centered-cubic crystal structure, the atoms at the (001) surface define a surface plane with C_{4v} symmetry. The corresponding surface Brillouin zone for the Cr(001) surface electronic structure is a square, as shown in Fig. 2. We assign k_{\parallel}^f (\AA^{-1}) values (along [010]) to the surface features observed in our ARPES spectra via the equation⁵

$$k_{\parallel}^f = 0.512(h\nu - E_{\text{IN}} - \phi)^{1/2} \sin\theta_e, \quad (3)$$

where ϕ is the Cr(001) work function (4.6 eV). For $k_{\parallel}^f \leq 1.09 \text{ \AA}^{-1}$ (the k_{\parallel} value of \bar{X}), $\mathbf{k}_{\parallel}^f = \mathbf{k}_{\parallel}$. For $k_{\parallel}^f > 1.09 \text{ \AA}^{-1}$, a nonzero value of \mathbf{g}_{\parallel} is used in Eq. (2) to relate \mathbf{k}_{\parallel}^f to \mathbf{k}_{\parallel} in the first surface Brillouin zone.

Figure 3 contrasts two normal-emission ($\theta_e = 0^\circ$) ARPES spectra of Cr(001) that use the p - and s -polarization geometries. The two surface-sensitive features reported previously¹⁴ are labeled 1 and 2 for the p -polarization spectrum 3(a). Since $\theta_e = 0^\circ$ for Fig. 3, $k_{\parallel} = 0 \text{ \AA}^{-1}$ for these photoelectron peaks. The features 1 and 2 therefore arise from initial states at the $\bar{\Gamma}$ point of

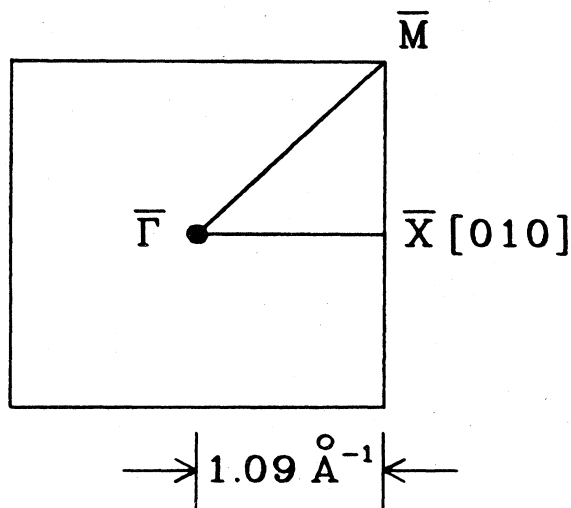


FIG. 2. The Cr(001) surface Brillouin zone. The zone is a square with side $2\pi/a$. The value of the lattice constant a is 2.884 \AA .

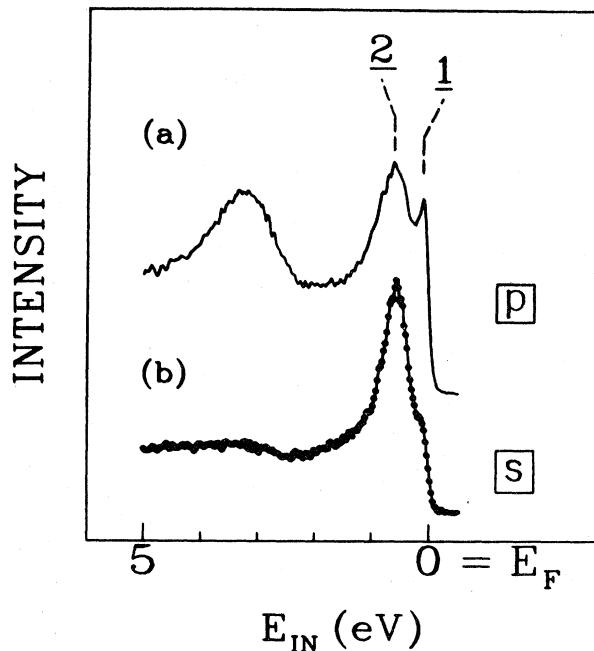


FIG. 3. The polarization dependence of the surface features 1 and 2. (a) Normal-emission ARPES spectrum of Cr(001) (at 298 K) using the p -polarization geometry. (b) Normal-emission spectrum in s polarization. The intensities of the spectra have been scaled to clarify the presentation.

the surface Brillouin zone. A subtle difference exists between spectrum 3(a) and the results reported previously.¹⁴ The binding energies that are observed in spectrum 3(a) for the surface features 1 and 2 are $E_{\text{IN}}(1) = 0.08(5) \text{ eV}$ and $E_{\text{IN}}(2) = 0.63(5) \text{ eV}$, respectively. These are both $\sim 0.12 \text{ eV}$ lower than the binding energies reported previously¹⁴ for ARPES spectra using synchrotron radiation of energy 23.00 eV. They are also $\sim 0.08 \text{ eV}$ lower than the E_{IN} values obtained with 21.2-eV synchrotron radiation from two independent experimental runs. The binding-energy discrepancies for $h\nu = 21.2 \text{ eV}$ are small. However, they are outside the experimental error with which E_{IN} is determined. Since the binding energy of the near-surface peak [$E_{\text{IN}} = 3.25(5) \text{ eV}$] in spectrum 3(a) is similarly affected, we attribute this systematic decrease in E_{IN} to a shift in the perceived spectroscopic position of the Fermi level, E_F . The origin of this shift is not understood at present. We believe that the results obtained with synchrotron radiation are intrinsically the more accurate due to the favorable spectroscopic conditions (absence of radiation satellites and low background pressure) for these measurements. Apart from this unexplained 0.08-eV shift in the derived E_{IN} values, the spectral properties of the surface features 1 and 2 that are revealed by 21.22-eV HeI_α ARPES measurements are identical to those observed using 21.2-eV synchrotron radiation.

The symmetry (group representation) of valence-band initial states may be directly obtained by exciting these electrons with polarized light and analyzing the resulting photoelectrons along a high-symmetry direction.⁶ For the

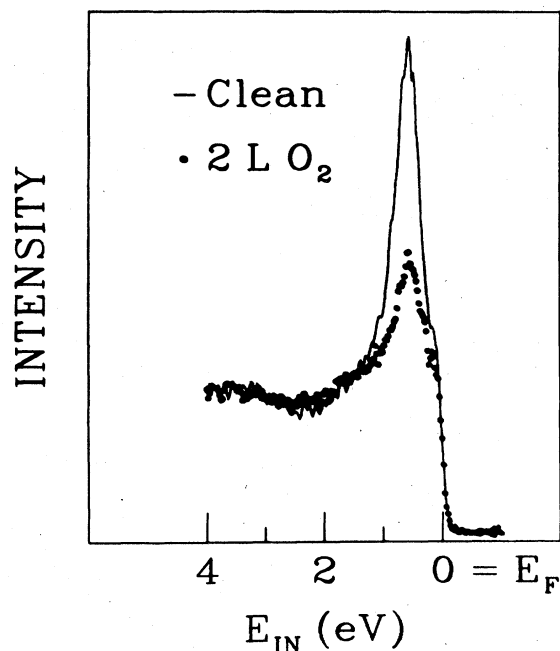


FIG. 4. Normal-emission s -polarization spectra of clean Cr(001) (line) and Cr(001) exposed to 2 L of oxygen (dots). The spectra have been normalized at $E_{IN}=3.0$ eV.

p -polarization normal-emission spectrum 3(a), only Δ_1 and Δ_5 initial states are allowed by dipole selection rules.⁶ Therefore the surface features 1 and 2 have either Δ_1 or Δ_5 symmetry at $\bar{\Gamma}$. That feature 1 has Δ_1 symmetry is shown by spectrum 3(b). For this s -polarization normal-emission spectrum, only Δ_5 initial states are allowed.⁶ The suppression of the surface feature 1 in spectrum 3(b) indicates that *the surface feature 1 possesses Δ_1 symmetry at $\bar{\Gamma}$* . Figure 4 reveals that the Δ_5 intensity of spectrum 3(b) is highly surface sensitive. The observations presented in Figs. 3 and 4 show that *the surface feature 2 possesses Δ_5 symmetry at $\bar{\Gamma}$* .

Figure 5 demonstrates that the surface features 1 and 2 display different spectral variations with $k_{||}$ along the $\bar{\Gamma}-\bar{X}$ line of the surface Brillouin zone (Fig. 2). As $k_{||}$ increases, photoelectron peak 2 disperses away from E_F with reduced spectral intensity. This behavior was also observed using the s -polarization geometry. In contrast, feature 1 does not disperse and loses less intensity than does feature 2 as $k_{||}$ is increased.

A high-intensity photoelectron peak dominates the ARPES spectrum for large values of θ_e . This prominent feature, referred to hereafter as feature 3, is observed to have a binding energy $E_{IN}(3)$ in the range $0.9 \geq E_{IN}(3) \geq 0.6$ eV for $1.0 \leq k_{||}^f \leq 2.0$ \AA^{-1} . A distinguishable feature-3 photoelectron peak is *not* observed at the corresponding lower values of θ_e for which $k_{||}^f = k_{||}$ in the first surface Brillouin zone. Figure 6 displays the sensitivity of feature 3 to surface contamination. Feature 3's photoelectron peak at $E_{IN}(3)=0.70(5)$ eV with $k_{||}^f=1.33(8)$ \AA^{-1} ($k_{||}=0.85$ \AA^{-1}) is strongly attenuated by exposing the Cr(001) surface to 1 L of CO (1 L=1 langmuir=

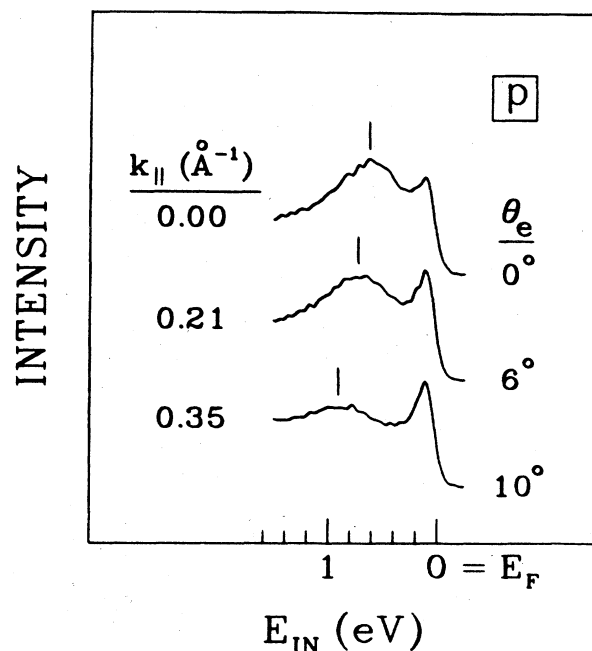


FIG. 5. ARPES p -polarization spectra of Cr(001) obtained by varying the angle of electron detection θ_e in the (100) mirror plane. The $k_{||}$ values are the wave-vector components parallel to the surface (along [010]) of the surface initial states responsible for the photoelectron peaks marked with a tic. The intensities of the spectra have been scaled for presentation.

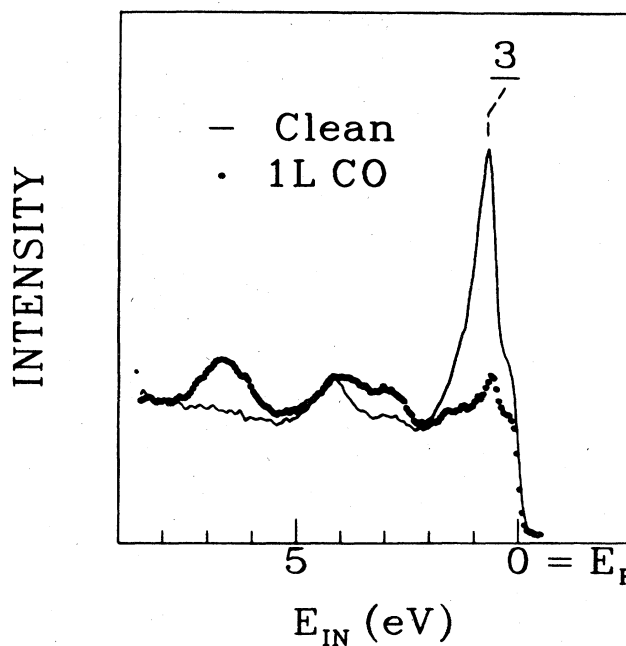


FIG. 6. Comparison of p -polarization ARPES spectra before (line) and after (dots) a 1-L CO exposure. The electron detection angle is 40.6° for both spectra. The contamination-induced peak at $E_{IN}=6.7$ eV is assigned to impurity (carbon and oxygen) $2p$ photoemission. The intensities of the two spectra have been normalized at $E_{IN}=8.0$ eV.

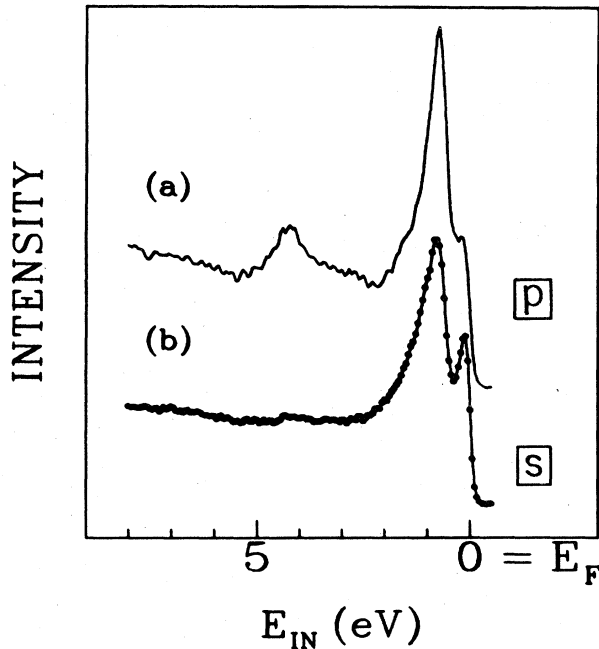


FIG. 7. The polarization dependence of feature 3. (a) p -polarization ARPES spectrum; $\theta_e = 40.6^\circ$. (b) Same as (a), only with s polarization. The intensities of the spectra have been scaled to clarify the presentation.

10^{-6} Torr sec). This suggests that the initial state 3 originates from the Cr(001) surface electronic structure.

The symmetry properties of the surface feature 3 are revealed in Fig. 7. The observation of the peak 3 in spectrum 7(a) (p polarization) indicates that feature 3 is even with respect to reflection through the (100) mirror plane. The persistence of surface-sensitive intensity in spectrum 7(b) (s polarization) suggests the existence of a surface feature that is odd with respect to (100) mirror-plane reflection. The binding energy of feature 3 in 7(b) is ~ 0.07 eV higher than that observed in 7(a). These findings reveal that *the surface feature 3 represents two nearly degenerate surface initial states of even and odd reflection symmetry at $k_{\parallel} = 0.85(8) \text{ \AA}^{-1}$.*

IV. THEORETICAL RESULTS AND DISCUSSION

The ARPES results of Sec. III characterize the surface electronic structure of Cr(001). The comparison of these results with theory provides insight into the magnetic properties of the Cr(001) surface. Previous theoretical investigations^{1-3,12} of the Cr(001) surface electronic structure calculated the k_{\parallel} -integrated SSDOS. In this section we report results from the first spin-polarized theoretical study of the symmetry, wave-vector and layer dependence of the Cr(001) surface electronic structure. Emphasis is placed on those results that can be compared directly to the photoemission measurements. A more complete description of the calculational method and general results for the Cr surfaces can be found in Ref. 18.

The faces of an 11-layer slab are used to represent the Cr(001) surface. The Hamiltonian is expressed in a basis consisting of $4s$, $4p$, and $3d$ orbitals. The one-electron term of the Hamiltonian is written in the Slater-Koster¹⁹ parametrized tight-binding scheme in which the one- and two-center integrals are fitted to the bulk band structure. The electron-electron interaction is limited to contributions from orbitals all centered on the same site and is treated in the Hartree-Fock approximation.¹⁸

The inclusion of $4s$ and $4p$ orbitals and a more accurate treatment of the electron-electron interaction should make the present calculation more accurate than previous tight-binding calculations of the Cr(001) surface electronic structure.^{1-3,12} Still, the use of a limited tight-binding basis set to represent surface states and resonances may lead to errors in the predicted energies of these features. The overall accuracy of our scheme can be judged from previous calculations for transition-metal systems in which our predictions for spin polarization²⁰ matched experiment and state-of-the-art calculations to within 0.1 electrons.^{8,21,22} Comparison of our calculated density of states with photoemission data also shows good agreement.²³ However, calculated ground-state binding energies tend to be larger than those observed in ARPES measurements. This is due in part to the influence of many-body processes on the photoelectric excitation.^{24,25} Recent ARPES studies^{26,27} of Cr(001) reveal that in certain regions of k space the spectroscopically observed $E_{IN}(k_i)$ are as much as 30% narrower than those predicted theoretically.²⁸

In agreement with previous theoretical studies,^{1-3,12} our calculations predict the existence of a ferromagnetic Cr(001) surface phase characterized by a very large surface spin polarization. Our theoretical prediction for the Cr(001) surface and near-surface magnetization is portrayed²⁹ in Fig. 8. In this figure the diameter of an atom is proportional to the theoretical magnitude of the atom's spin polarization. We predict the Cr(001) surface spin polarization to be 3.00 electrons. This spin polarization is the largest our theory has predicted for a pure transition-metal surface. If the value 2.00 is assumed for chromium's electronic g factor,²⁰ then our predicted surface spin polarization is consistent with an experimental estimate¹⁴ of the Cr(001) surface magnetic moment,³⁰ $2.4(8)\mu_B$. The enhanced polarization is expected to penetrate deeply into the bulk, as shown in Fig. 8. The second and third layers have predicted spin polarizations of -1.56 and 1.00 electrons, respectively. The magnitudes of the near-surface magnetic moments are thus thought to deviate significantly from the maximum bulk magnetic moment $0.59\mu_B$. Though its magnetization is enhanced, the Cr(001) near-surface region is predicted to be antiferromagnetic (Fig. 8). This is in agreement with a recent photoemission study²⁶ and with previous theory.^{2,12} We emphasize that the layer-dependent magnetization of Fig. 8 is a *bona fide* surface effect, conceptually distinct from the spin-density wave that exists in bulk chromium.¹³ Theoretically, the Cr(001) near-surface magnetization is largely determined by the ferromagnetism of the Cr(001) surface.

Since the (001) surface plane has a magnetization that is

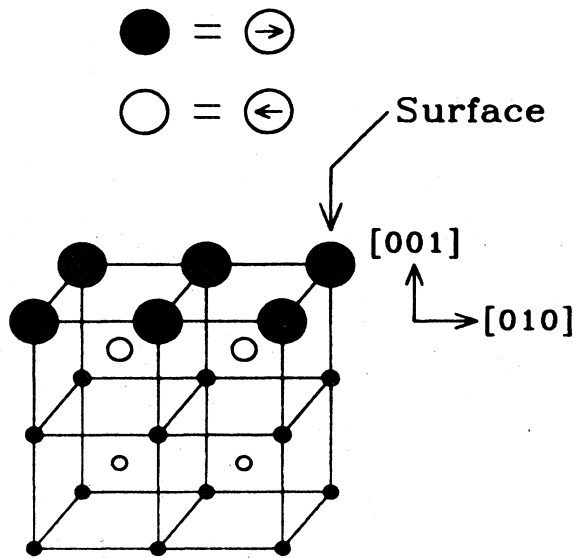


FIG. 8. Our theoretical prediction for Cr(001) surface and near-surface magnetism. Atoms whose magnetic moments point to the right are indicated by darkened spheres. Atoms whose magnetic moments point to the left are symbolized by open spheres. The diameter of the sphere representing an atom is drawn proportional to the magnitude of the atom's theoretical spin polarization. The surface spin polarization is predicted to be 3.00 electrons.

antiparallel to the magnetization of the second layer (Fig. 8), the theory predicts surface electronic states that are concentrated on either the surface or the second atomic layer. When the layer dependence of the Cr(001) surface electronic structure is discussed, the terms "majority spin" and "minority spin" become ambiguous. We use the label (+)-spin in reference to electrons with spin magnetic moment oriented parallel to the magnetization of the surface layer. Electrons whose moments lie antiparallel to the surface magnetization (but parallel to the second-layer magnetization) are labeled (-)-spin electrons. At the surface, a majority of the electrons have (+)-spin character. The opposite is true for the second layer.

The theoretical surface- and second-layer Cr(001) electronic structures at $\mathbf{k}_{\parallel}=0$ ($\bar{\Gamma}$) are shown in Figs. 9(a) and 9(b), respectively. Figure 9(a) shows a Δ_1 -symmetry (+)-spin surface resonance at 3.39 eV binding energy. This is accompanied by a Δ_1 -symmetry (-)-spin surface state at 2.86 eV binding energy that is localized on the second layer [Fig. 9(b)]. Both of these initial states have primarily d_{z^2} -orbital character with a small contribution from s and p orbitals. Closer to E_F , we predict two very strong surface states of Δ_5 symmetry and d_{xz} -, d_{yz} -orbital character. These states exist in a Δ_5 -symmetry gap of the surface-projected antiferromagnetic band structure. The (+)-spin state has binding energy 1.29 eV in Fig. 9(a), while the (-)-spin state is located 1.20 eV below (to the left of) E_F in Fig. 9(b). Note that a surface state is *not* predicted to exist in a theoretical²⁸ magnetically induced Δ_5 -symmetry gap at ~ 0.4 eV below E_F . A small Δ_1 -

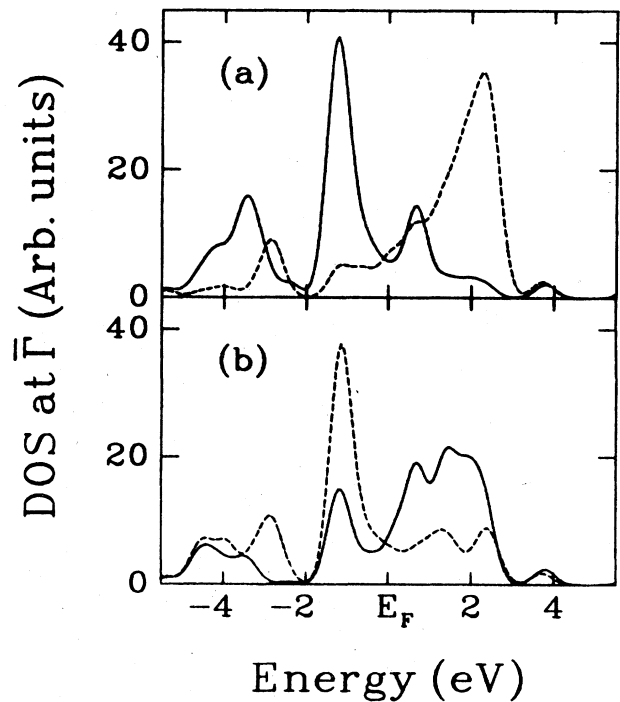


FIG. 9. The total ($4s+4p+3d$) theoretical Cr(001) (a) surface-layer and (b) second-layer density of states (DOS) at $\bar{\Gamma}$. The (+)-spin surface electronic structure is indicated by a solid line. The (-)-spin electronic structure is drawn with a dashed line. The theory has been broadened in energy by a 0.60 eV Gaussian to simulate experiment. States to the left of E_F are occupied.

symmetry (+)-spin surface state of mostly d_{z^2} -orbital character is also predicted with energy 0.68 eV above (to the right of) E_F in Fig. 9(a). This feature differs from the initial states predicted below E_F in that a companion Δ_1 -symmetry (-)-spin surface state is not predicted for the second layer, Fig. 9(b).

We now evaluate the consistency of these theoretical predictions with the ARPES results. The Δ_1 -symmetry photoelectron peak at ~ 3.2 eV binding energy in spectrum 3(a) has been previously attributed to a nonsurface initial state because it shows negligible sensitivity to surface contamination.²⁶ Since this feature lies in the spectral region predicted for the Δ_1 -symmetry surface resonance and its accompanying surface state, our ARPES experiment cannot determine the existence of these surface features at $\bar{\Gamma}$.

There is photoemission evidence for the theoretical Δ_5 -symmetry surface states and the lower-energy Δ_1 -symmetry surface state at $\bar{\Gamma}$. We believe that the (+)-spin and (-)-spin Δ_5 -symmetry surface states in Fig. 9 correspond to the observed Δ_5 -symmetry surface feature 2. The nearly degenerate theoretical surface states have binding energies (~ 1.2 eV) near that observed for the surface feature 2 [$E_{IN}(2)=0.75(5)$ eV]. The discrepancy between the theoretical surface-state binding energies and

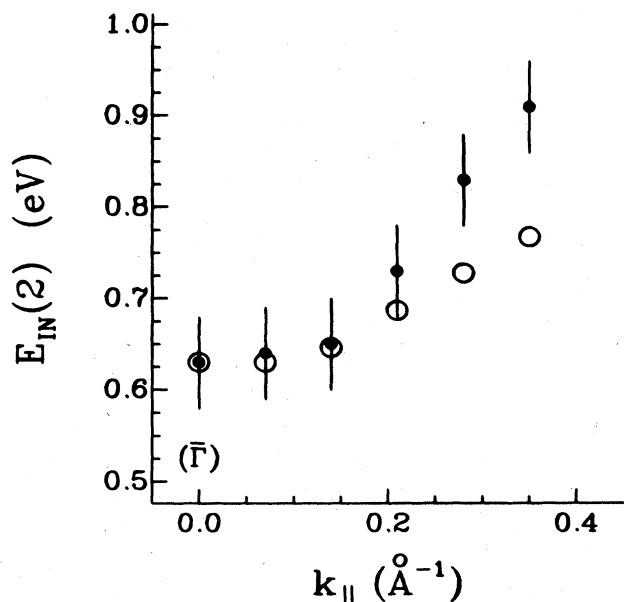


FIG. 10. The dispersion of the surface feature 2 along the $\bar{\Gamma}-\bar{X}$ line of the surface Brillouin zone observed using p -polarized HeI_{α} radiation. The open circles are adjusted theoretical values for the dispersion of the even-symmetry component of the Δ_5 -symmetry (+)-spin surface state. The theoretical binding energies were reduced by 0.66 eV so that experiment and theory agree at the $\bar{\Gamma}$ point.

$E_{IN}(2)$ may be due in part to the influence of many-body processes^{24,25} on the spectroscopic binding energies E_{IN} . The calculations predict that as $k_{||}$ increases along the $\bar{\Gamma}-\bar{X}$ line in the surface Brillouin zone (Fig. 2), the Δ_5 -symmetry surface states disperse in the same manner toward larger binding energies. The dispersion observed for the surface feature 2 in p -polarization HeI_{α} ARPES measurements is presented in Fig. 10. The open circles are adjusted theoretical values for the binding energy of the even-symmetry component of the (+)-spin Δ_5 surface state. This component is symmetry allowed in p polarization. The theoretical values were all reduced by 0.66 eV, so that the experimental and theoretical binding energies are equal at $\bar{\Gamma}$. Figure 10 demonstrates that the $k_{||}$ dependence of $E_{IN}(2)$ is similar to that predicted for the binding energy of the theoretical Δ_5 -symmetry surface states.

Figure 5 reveals that the surface feature 2 loses considerable spectroscopic intensity as $k_{||}$ increases along the $\bar{\Gamma}-\bar{X}$ line. This is consistent with the $k_{||}$ variation predicted for the even-symmetry component of the Δ_5 surface states. At $\bar{\Gamma}$ these theoretical surface features are *surface states* that are highly localized within the top two layers. As $k_{||}$ increases these surface states broaden into *surface resonances*. Accompanying this broadening is a delocalization of surface-resonance charge away from the surface. Since ARPES is intrinsically a surface-sensitive technique, a charge delocalization would reduce the spectral intensity of the Δ_5 surface features. This expectation is in agreement with the variation of the feature-2 intensi-

ty in Fig. 5. However, a quantitative explanation of the experimental intensities would require the calculation of photoelectric transition matrix elements.

Since the symmetry, binding energy, and spectral variation with $k_{||}$ of the surface feature 2 are consistent with the theory, we assign the *surface feature 2* to nearly degenerate Δ_5 -symmetry (+)-spin and (-)-spin surface states at $\bar{\Gamma}$. As such, feature 2 would have d_{xz} and d_{yz} orbital character. Note that this assignment predicts mixed spin polarization for the photoelectron peak 2. The preliminary assignment^{14,31} that was based on the theory of Allan¹ implied a (+)-spin character for feature 2.

Figure 3 demonstrates that the surface feature 1 possesses Δ_1 symmetry. The only Δ_1 -symmetry initial state near E_F is the theoretically unoccupied (+)-spin surface state located 0.68 eV above E_F in Fig. 9(a). The true energy position of this surface state may be closer to E_F than predicted. This possibility, combined with the very sharp onset of the feature-1 spectral intensity at E_F , leads us to assign the Δ_1 -symmetry *surface feature 1* to a *peaked spectral profile produced by the truncation of a Δ_1 -symmetry (+)-spin surface state by the Fermi level*. As such, feature 1 would have mostly d_{z^2} -orbital character. As $k_{||}$ increases along the $\bar{\Gamma}-\bar{X}$ line, the Δ_1 surface state is theoretically expected to lose less spectral intensity than the Δ_5 surface states (feature 2) because more of its charge remains surface localized. In addition, the Δ_1 surface state is predicted to disperse to lower energy with increasing $k_{||}$. This effect moves more of this state below the Fermi level, further enhancing the state's intensity, as $k_{||}$ increases. The persistent spectral intensity predicted for this Δ_1 surface state is consistent with the $k_{||}$ dependence of feature 1 in Fig. 5.

The assignment of feature 1 to the partial occupation of a (+)-spin surface state is similar to the previous interpretation¹⁴ of feature 1 that was based on the theory of Allan. However, that initial assignment attributed feature 1 to the occupation of the (-)-spin SSDOS. Our revised interpretation of feature 1 stated above suggests a predominantly (+)-spin character for feature 1.

Surface feature 3 is observed over the $k_{||}^f$ range $1.0 \leq k_{||}^f \leq 2.0 \text{ \AA}^{-1}$. This corresponds to a range of $k_{||}$ values $0.2 \leq k_{||} \leq 1.09 \text{ \AA}^{-1}$ in the first surface Brillouin zone. Recall from Sec. III and Fig. 7 that at $k_{||} = 0.85(8) \text{ \AA}^{-1}$ the surface feature 3 is composed of two nearly degenerate components that are even and odd with respect to reflection through the (100) mirror plane. The binding energies of the even and odd components in Fig. 7 were observed to be 0.72(5) and 0.80(5) eV, respectively. These properties are partially consistent with the theoretical results for the Cr(001) surface electronic structure along the $\bar{\Gamma}-\bar{X}$ line. At $k_{||} = 0.85 \text{ \AA}^{-1}$ theory predicts the existence of an even-symmetry surface resonance at 0.68 eV. Several odd-symmetry surface resonances are also predicted from 1.0–1.5 eV below E_F . However, these resonances are not strong features in the theory because they are broadened in energy and have much of their charge delocalized away from the surface. From a theoretical viewpoint the large spectral intensity observed for each component of the surface feature 3 is surprising.

Since k_{\perp} is not a good quantum number for the surface

electronic structure, the binding energy of a surface state or resonance should be independent of k_{\perp} and therefore $h\nu$. The $E_{\text{IN}}(2)$ values obtained using many different energies of synchrotron radiation were observed to lie in the range $0.70(5) \leq E_{\text{IN}}(2) \leq 0.80(5)$ eV. We do not interpret this range of E_{IN} as definitive evidence that $E_{\text{IN}}(2)$ varies with $h\nu$ and therefore k_{\perp} . It may be that nonsurface initial states can produce low-intensity photoelectron peaks near $E_{\text{IN}}(2)$. Since these can disperse with k_{\perp} , the apparent mean of the surface feature 2 might change slightly with $h\nu$, as is observed. The mean of the peaked spectral profile that we have labeled feature 1 shows no dependence on $h\nu$. The k_{\perp} dependence of the surface feature 3 was not investigated.

V. RELATIONSHIP TO PRIOR EXPERIMENTAL WORK

Gewinner *et al.*²⁷ first reported the surface feature 2 in the course of their room-temperature ARPES investigations of Cr(001) electronic structure. Using unpolarized HeI_{α} radiation, they report $E_{\text{IN}}(2)$ to be 0.65 eV, in agreement with our helium-lamp ARPES measurements. However, Gewinner *et al.* assign Δ_1 symmetry to feature 2, and attribute its origin to a Δ_1 -symmetry gap in the paramagnetic bulk band structure.²⁷ Later, Aitelhabti *et al.*³² reinterpreted the data of Gewinner and co-workers.²⁷ They concluded that the photoelectron peak 2 did not possess pure Δ_1 character, but also contained a smaller component of Δ_5 symmetry. They speculated that the observed spectral intensity was produced by photoemission from a Δ_5 -symmetry d -band edge and a Δ_1 -symmetry surface state or resonance.³² These previous ARPES investigations did not report the surface features 1 or 3.

The ARPES results presented here have shown that the surface feature 2 possesses Δ_5 symmetry, not Δ_1 symmetry as reported previously.^{27,32} The incorrect symmetry assignments made in the previous investigations are probably caused by the use of unpolarized HeI_{α} radiation in those measurements. Both theory (Fig. 8) and experiment²⁶ indicate that the Cr(001) near-surface region is antiferromagnetic. It was therefore conceptually incorrect for the previous workers^{27,32} to view the Cr(001) surface electronic structure using a surface-projected paramagnet-

ic bulk band structure. The discussion of the Cr(001) surface electronic structure should incorporate a surface-projected antiferromagnetic Cr band structure, as done in the present work.

VI. CONCLUSIONS

We conclude by recalling the major results of this work. Two surface-related photoemission peaks (features 1 and 2) are observed in normal-emission ARPES spectra of Cr(001). The symmetry, binding energy, and spectral variation with k_{\parallel} of each feature are consistent with results from a comprehensive spin-polarized calculation of Cr(001) surface electronic structure. Feature 2 is interpreted as two nearly degenerate Δ_5 -symmetry (+)-spin and (-)-spin surface states at $\bar{\Gamma}$. Feature 1 is attributed to the population of a Δ_1 -symmetry (+)-spin surface state at $\bar{\Gamma}$ with Fermi-Dirac statistics. The theory predicts a ferromagnetic Cr(001) surface phase characterized by a very large (3.00 electrons) surface spin polarization. We interpret the overall agreement between experiment and theory as evidence that the Cr(001) surface is, in fact, ferromagnetic. This conclusion is supported by a recent temperature-dependent ARPES investigation¹⁴ of Cr(001).

Two nearly degenerate surface initial states of even and odd reflection symmetry (feature 3) were observed at $k_{\parallel} = 0.85 \text{ \AA}^{-1}$ along the $\bar{\Gamma}-\bar{X}$ line. The existence of these features is partially consistent with the theoretical predictions. However, the large spectral intensity observed for these photoelectron peaks is poorly understood.

ACKNOWLEDGMENTS

The experimental work was supported by the Director, Office of Energy Research, Office of Basic Energy Sciences, Chemical Sciences Division of the U. S. Department of Energy, under Contract No. DE-AC03-76SF00098. The theoretical work was supported by the Director, Office of Basic Energy Sciences, Materials Sciences Division of the Department of Energy, under Contract No. DE-AC03-76SF00098. One of us (R.H.V.) would like to acknowledge the support of AT&T Bell Laboratories, under whose sponsorship this work was done.

¹G. Allan, *Surf. Sci.* **74**, 79 (1978).

²G. Allan, *Phys. Rev. B* **19**, 4774 (1979).

³G. Allan, *Surf. Sci. Rep.* **1**, 121 (1981).

⁴Z. Hussain, S. Kono, L.-G. Petersson, C. S. Fadley, and L. F. Wagner, *Phys. Rev. B* **23**, 724 (1981), and references therein.

⁵G. D. Mahan, *Phys. Rev. B* **2**, 4334 (1970).

⁶J. Hermanson, *Solid State Commun.* **22**, 9 (1977).

⁷S. Ohnishi, A. J. Freeman, and M. Weinert, *Phys. Rev. B* **28**, 6741 (1983).

⁸R. H. Victora, L. M. Falicov, and S. Ishida, *Phys. Rev. B* **30**, 3896 (1984).

⁹E. Wimmer, A. J. Freeman, and H. Krakauer, *Phys. Rev. B* **30**,

3113 (1984).

¹⁰A. M. Turner and J. L. Erskine, *Phys. Rev. B* **30**, 6675 (1984), and references therein.

¹¹J. L. Erskine, *Phys. Rev. Lett.* **45**, 1446 (1980), and references therein.

¹²D. R. Grempel, *Phys. Rev. B* **24**, 3928 (1981).

¹³G. Shirane and W. J. Takei, *J. Phys. Soc. Jpn.* **17**, Suppl. B III, 35 (1962).

¹⁴L. E. Klebanoff, S. W. Robey, G. Liu, and D. A. Shirley, *Phys. Rev. B* **30**, 1048 (1984).

¹⁵S. D. Kevan and D. A. Shirley, *Phys. Rev. B* **22**, 542 (1980).

¹⁶We adopt the gauge such that the electric field $E(\mathbf{r}, t)$ is relat-

- ed to the vector potential $A(\mathbf{r},t)$ via the relation $E(\mathbf{r},t)=(i\omega/c)A(\mathbf{r},t)$: K. L. Kliewer, in *Photoemission and the Electronic Properties of Surfaces*, edited by B. Feuerbacher, B. Fitton, and R. F. Willis (Wiley, New York, 1978), p. 47.
- ¹⁷A. G. Baca, L. E. Klebanoff, M. A. Schulz, E. Paparazzo, and D. A. Shirley (unpublished).
- ¹⁸R. H. Victora and L. M. Falicov, *Phys. Rev. B* **31**, 7335 (1985).
- ¹⁹J. C. Slater and G. F. Koster, *Phys. Rev.* **94**, 1498 (1954).
- ²⁰The spin polarization P (electrons) may be accurately related to the magnetic moment M (μ_B) if the electronic g factor is known: $M = Pg/2$.
- ²¹R. H. Victora and L. M. Falicov, *Phys. Rev. B* **30**, 259 (1984).
- ²²J. Tersoff and L. M. Falicov, *Phys. Rev. B* **26**, 6186 (1982).
- ²³R. H. Victora and L. M. Falicov, *Phys. Rev. B* **28**, 5232 (1983).
- ²⁴L. Ley, F. R. McFeely, S. P. Kowalczyk, J. G. Jenkin, and D. A. Shirley, *Phys. Rev. B* **11**, 600 (1975).
- ²⁵L. Ley, S. P. Kowalczyk, F. R. McFeely, R. A. Pollak, and D. A. Shirley, *Phys. Rev. B* **8**, 2392 (1973).
- ²⁶L. E. Klebanoff, S. W. Robey, G. Liu, and D. A. Shirley, *Phys. Rev. B* **31**, 6379 (1985).
- ²⁷G. Gewinner, J. C. Peruchetti, A. Jaéglé, and R. Pinchaux, *Phys. Rev. B* **27**, 3358 (1983).
- ²⁸H. L. Skriver, *J. Phys. F* **11**, 97 (1981).
- ²⁹Figure 8 is similar to Fig. 17 of Ref. 26. However, that previous figure depicted the near-surface Cr(001) magnetization as predicted by Allan (Ref. 2).
- ³⁰The arguments made in Ref. 14 to infer the Cr(001) surface magnetic moment M_s assume a g factor of 2.00. Also, the error bars reported in Ref. 14 ($\pm 0.3\mu_B$) for M_s are incorrect. The M_s uncertainty quoted in the present work ($\pm 0.8\mu_B$) is estimated from the error associated with $E_{IN}(2)$ and possible errors resulting from the use of an approximate model to infer M_s .
- ³¹In the previous report (Ref. 14), the feature 2 was tentatively labeled a surface resonance. The present work suggests that this identification may not be correct.
- ³²D. Aitelhabeti, G. Gewinner, J. C. Peruchetti, R. Riedinger, D. Spanjaard, and G. Tréglia, *J. Phys. F* **14**, 1317 (1984).